

# PCCP

Accepted Manuscript



This is an *Accepted Manuscript*, which has been through the Royal Society of Chemistry peer review process and has been accepted for publication.

*Accepted Manuscripts* are published online shortly after acceptance, before technical editing, formatting and proof reading. Using this free service, authors can make their results available to the community, in citable form, before we publish the edited article. We will replace this *Accepted Manuscript* with the edited and formatted *Advance Article* as soon as it is available.

You can find more information about *Accepted Manuscripts* in the [Information for Authors](#).

Please note that technical editing may introduce minor changes to the text and/or graphics, which may alter content. The journal's standard [Terms & Conditions](#) and the [Ethical guidelines](#) still apply. In no event shall the Royal Society of Chemistry be held responsible for any errors or omissions in this *Accepted Manuscript* or any consequences arising from the use of any information it contains.

## Reactivity of the free and (5,5)-carbon nanotube supported AuPt bimetallic clusters towards O<sub>2</sub> activation. A theoretical study

Fazel Shojaei<sup>1</sup>, Masoumeh Mousavi<sup>1</sup>, Fariba Nazari<sup>1,2</sup>, Francesc Illas<sup>3</sup>

<sup>1</sup>*Department of Chemistry, Institute for Advanced Studies in Basic Sciences, Zanjan 45137-66731, Iran*

<sup>2</sup>*Center of Climate Change and Global Warming, Institute for Advanced Studies in Basic Sciences, Zanjan 45137-66731, Iran*

<sup>3</sup>*Departament de Química Física & Institut de Química Teòrica i Computacional (IQTCUB), Universitat de Barcelona, C/Martí i Franquès 1, 08028 Barcelona, Spain*

### Abstract

Density Functional Theory (DFT) based calculations have been carried out to predict the geometry, energy and electronic structures of the small bimetallic Au<sub>m</sub>Pt<sub>n</sub> (2 ≤ m+n ≤ 4) clusters deposited on a single-wall (5-5)-carbon nanotube (CNTs). The chemical reactivity of these supported bimetallic clusters towards O<sub>2</sub> reduction reaction is also considered. The calculations indicate that Au atoms tend to avoid the CNT atoms whereas the opposite occurs for Pt atoms, a behavior which can be rationalized through analyses of the density of states plots. Compared to isolated clusters, the supported counterparts are found to have a significant superiority in catalytic activity towards O<sub>2</sub> reduction. The adsorption configuration and identity of the metal (Au or Pt) exposed to the O<sub>2</sub> molecule adsorption are the dominant factors in determining the catalytic activity of the supported particles. Most notably, the high catalytic activity of the supported-clusters is associated with a drastic decrease in adsorption energy of the O<sub>2</sub> molecule.

**Keywords:** carbon nanotube (CNT), O<sub>2</sub> reduction, Au/Pt bimetallic clusters, catalytic activity,

## Introduction

Two existing pre-market proton exchange membrane fuel cells (PEMFCs) have been identified as highly-efficient electrochemical converter either using hydrogen or methanol as fuel.<sup>1-3</sup> The low emissions and friendly environmental properties of these PEMFCs strongly suggest that these may constitute alternative “green” power sources in the near future. The overall chemical reaction consists simply of hydrogen oxidation ( $\text{H}_2 \rightarrow 2\text{H}^+ + 2\text{e}^-$ ) at the anode and oxygen reduction ( $\frac{1}{2} \text{O}_2 + 2\text{H}^+ + 2\text{e}^- \rightarrow \text{H}_2\text{O}$ ) at the cathode.

The electrochemical reactions in PEM fuel cells do seem and, in fact, are simple but require a proper electrocatalyst. Among the possible and suitable nanostructured electrocatalysts, Pt or Pt-alloyed nanoparticles are still the most effective ones being able to simultaneously assist both, oxygen reduction and hydrogen (or alcohol) oxidation even though with very different reaction rates.<sup>4-6</sup> Despite the unique properties of Pt nanostructured electrocatalyst, the high-cost and scarcity of this element continues to constitute a serious bottleneck for a widespread use of PEMFCs. Other two main obstacles are the strong adsorption of some intermediates such as CO in the anode which is unavoidable when hydrogen is derived from an alcohol or hydrocarbon fuel<sup>7-9</sup> and formation of the large proportion of  $\text{H}_2\text{O}_2$  in the cathode<sup>10-13</sup> which both poison the catalyst. The poor oxygen reduction kinetics at the cathode severely limits energy conversion in PEMFCs.. However, finding an alternative to Pt as catalyst which would have similar performance of Pt in both anodic and cathodic processes is not an easy task.

Combining Pt with other transition metals such as Ni, Co, Fe, Ti, or V resulting in different types of bimetallic alloys has been largely explored from both experimental<sup>14-26</sup> and computational modeling<sup>27-33</sup> viewpoints. Alloying with less active, more noble metals, such as Ru, Pd, and Ag has been also considered.<sup>34-38</sup> Nevertheless, it is worthwhile mentioning that “long-term durability” constitutes a major challenge for application of alloys involving Pt and transition metal as electrocatalysts. In many cases, the transition metal element is degraded over operation of the system as reported for PtCo/C cathode catalysts.<sup>39,40</sup> For this reason, the Au/Pt combination is still considered a special case attracting a great deal of attention. One of the most characteristic features of Au is its higher oxidation potential compared to Pt which naturally makes Au/Pt combination a proper alternative catalyst. Recently, synthesized Au/Pt nanoparticles have exhibited superior catalytic activities for  $\text{O}_2$  reduction and CO oxidation which have obvious advantages over Pt and other Pt-based nanomaterials.<sup>41-43</sup> Note in passing by that, Au at nanoscale has remarkable catalytic activities<sup>44-46</sup> and many related studies have been published in the recent years.<sup>47-52</sup> Note also

that many recent studies have substantiated that nanosized Au-based catalysts are the best candidates for the water gas shift (WGS) reaction ( $\text{CO} + \text{H}_2\text{O} \rightarrow \text{H}_2 + \text{CO}_2$ ), and also for CO oxidation ( $2\text{CO} + \text{O}_2 \rightarrow 2\text{CO}_2$ ) at low temperatures.<sup>53,54</sup> These two reactions are indeed used to reduce the concentration of CO in H<sub>2</sub> supplies to PEMFCs. The unique properties of nano-Au have stimulated several experimental works aimed at synthesizing bimetallic Au/Pt electrocatalysts which employ a variety of different approaches.<sup>43,51-66</sup> Interestingly, Zhang et al.<sup>67</sup> reported that the Au-modified Pt electrocatalyst working as a cathode is stabilized against dissolution (formation of Pt-OH and Pt-O and its consequent surface corrosion) under highly oxidizing conditions and potential cycling regimes. In contrast to the pure Pt catalyst, the morphology of the new catalyst remains almost unchanged without degrading the oxygen reduction kinetics.

The choice of the support constitutes an additional challenge since it is clear that the nature of the support greatly influences the catalytic behavior of the metallic nanoparticles. For instance, it has been recently shown that the catalytic activity of Pt nanoparticles towards the WGS reaction is greatly enhanced over deposition on CeO<sub>2</sub>, a clear cut case of beneficial strong metal-support interaction.<sup>68</sup> The role of the support is not limited to oxides, transition metal carbides such as TiC have been shown to activate supported Au nanoparticles because of the C ↔ Au interaction.<sup>69</sup> Recently, it has been reported that Au/TiC is especially active for the WGS reaction performing even better than Au/TiO<sub>2</sub> or Cu/ZnO.<sup>70</sup> The role of the C ↔ Au interaction on the catalytic performance of Au/TiC strongly suggests that C supports may be a good choice for AuPt bimetallic nanoparticles too. Moreover, the large surface area of carbon supports provide a convenient condition to design electrocatalysts with, ideally, the lowest possible precious metal loading and, at the same time, the highest activity and durability, simply because, in principle, metal catalyst particles can be dispersed to a high degree. Among the various carbon allotropes,<sup>71,72</sup> the remarkable properties of carbon nanotubes (CNTs) make these fascinating systems potentially good candidates as useful and effective supports for these nanoscale precious metals. In his review article, Antolini<sup>73</sup> describes how the performance of several Pt-based catalysts supported on carbon is influenced by the factors such as surface area, electron conductivity, porosity, corrosion resistance and morphology of the catalyst layer durability. The results of Luo et al.<sup>62</sup> revealed that the activity of carbon-supported Au/Pt catalysts in the oxygen reduction reaction (ORR) does not only depend on the alloy composition but also on the nature of the electrolyte. An alternative explanation of the activity of both cathode and anode, based on the

nature of electrolyte (acidic and alkaline) and composition, has been presented by Tang et al.<sup>65</sup>

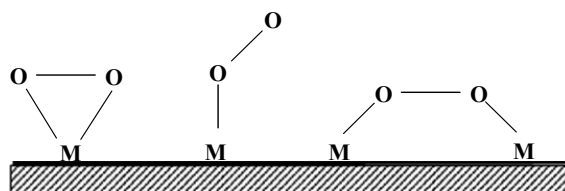
From a computational perspective, a great deal of effort has been devoted to describe the interactions of bare or carbon-supported Pt or Au small nanoparticles with various simple molecules like O<sub>2</sub>.<sup>74-82</sup> Precisely, the effect of particle size on the dissociation of O<sub>2</sub> has been also investigated including particles containing up to 225 atoms.<sup>83,84</sup> In Au/Pt binary alloys, however, theoretical investigations are limited either to the case of bare small clusters or to the study of extended surfaces.<sup>85,86</sup> Regarding, Au/Pt supported bimetallic particles, the only available study involves the interaction of binding of Au<sub>m</sub>Pt<sub>n</sub> (m=1-3) on a carbon-support.<sup>87</sup> Clearly, a systematic examination on the atomic and electronic structure of carbon supported Au/Pt clusters as well as their interaction with O<sub>2</sub> will provide useful information regarding this potentially useful type of electrocatalyst. In this work, we aim precisely at presenting a complete picture of the behavior of bimetallic small Pt/Au clusters supported on CNTs which can be considered as model systems. Hence, bimetallic Au<sub>m</sub>Pt<sub>n</sub> (2≤m+n≤4) clusters supported on single-wall (5-5)-carbon nanotube are chosen as model catalysts to investigate the O<sub>2</sub> reduction reaction and other properties of interest. . Our calculations would be based on density functional theory (DFT). Through a comparative study, we will provide evidence on how and when bimetallic formation on a carbon-support modifies or even destroys the catalytic activity of the system towards ORR. From the analysis of energetic, electronic and geometrical parameters obtained in the absence and in the presence of the carbon-support, we establish a correlation between the various adsorption patterns and binding energy as well as of the catalytic activity of the supported nanoparticle.

### Computational details and materials models

The adsorption of Au<sub>m</sub>Pt<sub>n</sub> (2≤m+n≤4) clusters on the surface of pristine (5-5)-CNT is studied by means of spin polarized density functional theory based (sDFT) calculations with the PBE form of the Generalized Gradient Approach (GGA) exchange-correlation functional<sup>88</sup> as implemented in Quantum ESPRESSO.<sup>89</sup> This GGA functional provide the most balanced description for the series of 30 transition metal elements.<sup>90</sup> The valence electron density has been expanded in a plane wave basis set with a sufficiently high cutoff for the kinetic energy. The effect of the core electrons on the valence density (electron-ion) interaction is described through ultrasoft pseudopotentials (US-PP).<sup>91,92</sup> At first step, structural optimization of the bare metallic clusters and O<sub>2</sub>adsorption complexes is carried out in a cubic box with dimension of approximately 10 Å, using cutoff energy of 448 eV for the plane wave and, obviously, using the reciprocal space gamma point only. For the Au<sub>m</sub>Pt<sub>n</sub>

clusters, the interaction with the O<sub>2</sub> molecule results in a coverage of 2/(n+m) with respect to the total number of exposed surface atoms. An energy threshold of 10<sup>-8</sup> a.u. is used for self-consistency, whereas for geometry optimizations, the applied convergence criteria were 10<sup>-3</sup> a.u. on the forces acting on each atom.

Using the notation introduced by Yeager et al.<sup>93,94</sup>, we consider three adsorption modes for associative adsorption of O<sub>2</sub> on the surface metal catalyst which are schematically shown in Scheme 1 and discussed at length in Ref. 95. In short, these three modes are: 1) O<sub>2</sub> is placed on top of one metal atom (Griffith mode), 2) end-on adsorption through a single bond (Pauling mode) and, 3) O<sub>2</sub> bridges over two metal atoms while the O–O axis is parallel to the metal-metal axis (Yeager or bridge mode).



**Scheme 1.** The three major adsorption modes for O<sub>2</sub> on metal surfaces

The binding energy per atom of the naked bimetallic Au<sub>n</sub>Pt<sub>m</sub> clusters is obtained as in eqn 1a

$$E_b = - [E(\text{Au}_n\text{Pt}_m) - (nE(\text{Au}) + mE(\text{Pt}))] / (m + n) \quad (1a)$$

whereas eqns 1b and 1c below provide the energy of adding one Au or Pt atom to the Au<sub>n-1</sub>Pt<sub>m</sub> or Au<sub>n</sub>Pt<sub>m-1</sub> cluster, respectively

$$E_{int}^M(\text{Au}_n\text{Pt}_m) = - [E(\text{Au}_n\text{Pt}_m) - (E(\text{Au}) + E(\text{Au}_{n-1}\text{Pt}_m))] \quad (1b)$$

$$E_{int}^M(\text{Au}_n\text{Pt}_m) = - [E(\text{Au}_n\text{Pt}_m) - (E(\text{Pt}) + E(\text{Au}_n\text{Pt}_{m-1}))] \quad (1c)$$

In a similar way, the interaction of the oxygen molecule with the isolated cluster is calculated as in eqn (2)

$$E_b = - [(E(\text{Au}_n\text{Pt}_m\text{O}_2) - (E(\text{Au}_n\text{Pt}_m) + E(\text{O}_2)))] \quad (2)$$

The interaction of O<sub>2</sub> with the naked clusters and with the bare substrate has been studied by considering all possible adsorption modes. A similar systematic search has also been carried out to study the interaction of O<sub>2</sub> with the bimetallic particles supported on the (5-5) carbon nanotube. To have compromise between size and computational cost, to reduce the filling of CNT by choosing the smallest stable metallic CNT, (5,5)-CNT are chosen for this investigation. It should be emphasized that the metallic character of CNT is important because the designed catalyst is going to use as an electrocatalyst. In the case of the bare (5-5)

carbon nanotube, the three common adsorption sites (top, bridge and the center of hexagon ring)<sup>96,97</sup> have been investigated (Fig. 1).

For the optimized structures charge density difference (CDD) plots are used to help to recognize charge accumulation or depletion in different regions which is a useful reactivity descriptor. The CDD in different regions is calculated as in eqn ( 3),

$$\Delta\rho(r) = \rho(r)_{M(MO)-Su} - [\rho(r)_{Su} + \rho(r)_{M(MO)}] \quad (3)$$

where  $\rho(r)_{Su-M}$ ,  $\rho(r)_{Su}$  and  $\rho(r)_M$  are the charge density of the super-system, bare substrate and molecule, respectively. Density of the bare substrate and the molecule in eqn (3) are taken from the optimized super-system structure through single point calculations.

## Results and discussion

### *Structure and stability of the bare $Au_mPt_n$ clusters*

For comparative purposes, prior describing results regarding oxygen adsorption on bare or CNT supported bimetallic clusters we briefly describe the properties of the isolated  $Au_mPt_n$  clusters. At first step, the lowest energy configurations of the isolated  $Au_m$  ( $m=2-5$ ) and  $Pt_n$  ( $n=2-5$ ) clusters are considered. Next, a series of  $Au_mPt_n$  bimetallic clusters is constructed by simply substituting Au atoms with Pt until the pure platinum cluster is reached. It is worth mentioning that the small  $Au^{98-103}$ ,  $Pt^{104-109}$  and AuPt binary clusters<sup>103,110-114</sup> have been extensively studied. In particular, the role of composition on the geometrical structure in  $Au_mPt_n$  clusters with low nuclearity ( $2 \leq m+n \leq 5$ ) has been reported,<sup>111,115</sup> The present results are essentially in agreement with previous studies with some small differences arising from the use of slightly different computational setups. The results (Fig S1 to Fig. S9) and detailed explanations are given in supplementary file.

### *3.2 Atomic and electronic structure of the (5-5) CNT- supported $Au_m$ , $Pt_m$ and $Au_nPt_m$ clusters*

For the armchair nanotubes, the four high symmetry sites displayed in Fig. 1 are considered as possible active sites for anchoring metallic clusters. The lowest energy configurations for  $Au_mPt_n$  ( $2 \leq m+n \leq 4$ ) nanoparticles adsorbed on the(5-5) CNT have been found after a systematic search. The lowest energy structures are displayed in Figure 2 where the adsorption energy,  $E_{ads}$ , calculated as in eqn ( 4)

$$E_{ads} = E_{AuPt/CNT} - (E_{CNT} + E_{Au/Pt}) \quad (4)$$

is also included. In this definition  $E_{AuPt/CNT}$  refers to the  $Au_mPt_n/CNT$  adsorption complex and  $E_{CNT}$  and  $E_{Au/Pt}$  refer to the energies of free CNT and  $Au_mPt_n$  moieties, respectively.

The ground state properties of carbon supported  $Au_n$  ( $n=2-4$ )<sup>116-119</sup> as well as  $Pt_n$  ( $n=2-4$ )<sup>120-123</sup> clusters have been previously studied. In agreement with those works, the present results show that  $Au_2$  adsorbs preferentially in a vertical orientation at the  $B_{zigzag}$  site of CNT

(Fig. 2) with modest adsorption energy 0.90 eV. For the supported Pt<sub>2</sub> cluster, the preferred orientation is parallel to the C-C of B<sub>zigzag</sub> site with comparatively significantly larger adsorption energy (2.34 eV), although the vertical configuration is only 0.02 eV higher in energy. The Pt-Pt bond length for the adsorbed dimer is 2.60 Å, quite larger than that for the gas-phase cluster (2.33 Å). This contrasts with the case of the supported Au<sub>2</sub> for which the bond length is almost the same as in the gas phase. For the supported Au<sub>3</sub> and Pt<sub>3</sub> clusters, the upright isosceles triangle is a preferred structure although with a considerable difference in adsorption energy 1.04 eV and 3.21 eV, respectively. A quite small adsorption energy is the most obvious feature of the supported Au<sub>4</sub> (0.57 eV) shown in Fig. 1 with a structure close to that of the gas phase cluster. Here, an upright geometry with one Au atom coordinated to the top site of the CNT surface is still preferred as the most stable structure, which is in a close agreement with Li et al.<sup>117</sup>. The small adsorption energy and little distortion with respect to the gas phase cluster are in line with results for supported Au<sub>2</sub> and Au<sub>3</sub>. On the other hand, calculations predict a severe restructuring of the structure of the Pt<sub>4</sub> cluster upon adsorption on CNT, going from an almost planar geometry to a three-dimensional tetrahedron like shape at which one of the four triangular faces is directly placed above the CNT surface (two atoms on the top sites and one on the B<sub>axial</sub> site). The geometry of the CNT is also slightly disturbed upon Pt<sub>4</sub> adsorption with C-C bond lengths of the adsorption site elongated to 1.46 Å for both B<sub>axial</sub> and B<sub>zigzag</sub> sites. Clearly, Pt-support interactions are much stronger than those for Au-support.

Let us now turn our attention to the structure of the supported bimetallic clusters. The lower affinity of Au atoms towards the carbon surface suggests that adsorption of Au<sub>m</sub>Pt<sub>n</sub> on CNT takes place through the Pt atoms. This is confirmed by systematic calculations showing that Au/Pt clusters adsorb on the CNT always via Pt atoms (see also supporting information file). In the case of PtAu, an upright geometry with the Pt atoms in contact with the surface corresponds to the most favorable conformation. Not unexpectedly, the substitution of Au atoms with Pt results in a larger adsorption energy which increases with Pt concentration in the bimetallic cluster (Fig. 2). It is worth pointing out that the rather weak interaction of Au clusters with CNT does not affect its atomic structure. However, the strong adsorbate-surface interaction between AuPt clusters and CNT leads to the strong disturbing of both geometries of the adsorbed nanoparticles and the initial surface of CNT. For instance, for the Au<sub>2</sub>Pt<sub>2</sub> cluster, the gas phase planar rhombus structure changes to a three dimensional tetrahedron-like one when Au<sub>2</sub>Pt<sub>2</sub> adsorbed on CNT with the Pt atoms at the B<sub>zigzag</sub> sites of the CNT. In some cases like in the supported AuPt<sub>3</sub>, the restructuring of the cluster and of the CNT is



much severe with a concomitant elongation of the Pt-Pt bond near the surface from 2.49 Å in the gas phase to 2.76 Å in supported form. This is in line with the results commented above for the Pt<sub>n</sub> supported clusters. The range of metal-C distances for the most stable supported clusters is reported in Fig. 3 which clearly shows that C-Au distances are always larger than Pt-C ones.

To complete the study of the supported metallic and bimetallic clusters we present a detailed analysis of the electronic structure based on Bader charges,<sup>124-125</sup> charge density difference, band structures and projected density of states (PDOS). The Bader charges on each atom and the magnitude of charge exchanged between the CNT and supported clusters ( $\Delta q$ ) are collected in Table 1, binding energies are included for comparison. The positive and the negative values represent charge depletion and accumulation, respectively,  $\Delta q$  indicates the final net Bader charge on CNT, and starred atoms refer to those which are directly in contact with the surface. Inspection of Table 1 reveals a clear correlation between the charge transfer and binding energy of the monometallic clusters so that the larger the charge transfer, the larger the cluster adsorption energy. For instance, in Pt<sub>4</sub>/CNT the highest net charge transfer ( $\Delta q=0.176$ ) correlates with the largest adsorption energy CNT ( $E_{\text{ads}}=-3.37$  eV). The same trend is observed in Au<sub>4</sub>/CNT, here one finds the smallest charge transfer ( $\Delta q=0.042$ ) and the smallest binding energy ( $E_{\text{ads}}=-0.57$  eV) values. This type of correlation has been also reported in previous works.<sup>124,126-128</sup> Another interesting feature emerging from Bader charges in Table 1 is that the metal atoms directly binding to the surface are always positively charged whereas the other ones are negatively charged. In the case of the Au/Pt bimetallic clusters, simple arguments based on electronegativity indicate that, in addition to the metal-carbon bond polarization, charge transfer will likely involve Pt which is in line with results in Table 1.

Additional information regarding the electronic structure of the supported clusters can be extracted from the band structures and DOS plots. Fig. 4 reports these plots for the simplest adsorption complexes (Au<sub>2</sub>/CNT, Pt<sub>2</sub>/CNT and AuPt/CNT). Let us recall that the armchair (5,5)-CNT exhibits a zero band gap and, hence, exhibits a metallic character. This character is still preserved in Pt<sub>2</sub>/CNT while for AuPt/CNT a tiny band gap already opens between  $\pi-\pi^*$  bands, slightly above the Fermi level. The crossing of  $\pi-\pi^*$  bands is a characteristic feature of armchair nanotubes which is easily recognized in the adsorption complexes. Significant differences in PDOS near the Fermi level are observed for Au<sub>2</sub>/CNT and Pt<sub>2</sub>/CNT systems. A clear change in the DOSs of C atoms is observed upon binding Pt<sub>2</sub> to the CNT. The Pt 5d and 6s states are mainly localized near the Fermi level facilitating their

interactions with C 2p states while Au derived states appear -0.8 eV below the Fermi level thus weakly interacting with the C 2p states. For the AuPt/CNT case, there is a substantial density of states at the vicinity of Fermi level dominated by Pt 5d orbitals as expected from the adsorption energy values. An obvious hybridization between C 2p states and Pt states is clearly observed as well. Here, the Au 5d and 6s states are closer to the Fermi level than those in Au<sub>2</sub>/CNT indicating a possible activation of Au in the supported AuPt bimetallic cluster.

*Oxygen adsorption on pure and bimetallic unsupported Au/Pt clusters*

The minimum energy structures with the lowest energy, corresponding binding energies, spin density, O-O and Au(Pt)-O bond distances found for adsorbed O<sub>2</sub> over pure and bimetallic Au<sub>n</sub>Pt<sub>m</sub> (2 ≤ m+n ≤ 5) clusters are shown in Fig. 5. To obtain the minimum structures with the lowest energy, a wide variety of possible initial geometries with different compositions (n/m) and multiplicities have been considered. Other low-lying minimum structures, their corresponding energy and geometrical parameters are reported in Fig. S11. The adsorption energy of the O<sub>2</sub> molecule on the bimetallic cluster, E<sub>ads</sub>, is computed as in eqn (5)

$$E_{\text{ads}} = E_{\text{AuPt/O}_2} - (E_{\text{O}_2} + E_{\text{cluster}}) \quad (5)$$

where E<sub>AuPt/O<sub>2</sub></sub>, E<sub>O<sub>2</sub></sub>, and E<sub>cluster</sub> are the total energies of adsorption complex, O<sub>2</sub> molecule and isolated Au<sub>m</sub>Pt<sub>n</sub> binary cluster, respectively. It is tempting to speculate how the mutual influence of different neighboring atoms leads to catalytic behavior which is considerably better than that of monometallic species.<sup>41-43</sup> Hence, a detailed analysis of adsorption of O<sub>2</sub> molecule on Au<sub>m</sub>, Pt<sub>m</sub> and Au<sub>m</sub>Pt<sub>n</sub> clusters is also presented. There are several articles devoted to understanding the different aspects of interaction between oxygen molecule and small pure Au<sup>108,141-132</sup> and Pt<sup>74,133-</sup> clusters. Therefore, only a brief description is provided for completeness. Figure 5 shows that among the four lowest energy structures of Au<sub>n</sub>/O<sub>2</sub> there is no structure corresponding to Griffith conformation. Pauling adsorption pattern is the most favored for interaction of O<sub>2</sub> with even-number Au<sub>m</sub> clusters (with singlet ground state), while odd-number Au<sub>m</sub> clusters (with doublet ground state) prefers Yeager pattern. Our calculations also confirm the familiar even-odd oscillation behavior in adsorption energy of O<sub>2</sub> over pure Au<sub>m</sub> clusters.<sup>83,84,108,130</sup> In the most stable structures, O-O and M-O bond distances found in present study for Au<sub>m</sub>/O<sub>2</sub> are in a good agreement with those reported by Mills et al.<sup>132</sup>. One of the most significant points in Fig. 5 is the very low values of adsorption energy for Au<sub>m</sub>/O<sub>2</sub> complexes. The weak interaction of O<sub>2</sub> with small gold clusters is mostly attributed to the significant HOMO-LUMO energy gap of Au clusters which cannot be

influenced effectively by the presence of O<sub>2</sub> molecule. Nevertheless, presence of unpaired valence electrons in odd-numbered Au<sub>n</sub> clusters make them more active towards O<sub>2</sub> molecule compared to even-number gold clusters, and their corresponding adsorption energies are comparatively higher. This larger adsorption energy is accompanied by the O-O bond length weakening, while the O-O bond length remains close to the equilibrium value for the isolated O<sub>2</sub> molecule (1.21Å) through the weak adsorption of O<sub>2</sub> on even-number gold clusters. In simple words, odd-numbered gold clusters are catalytically more active.

At variance of the situation encountered in the Au<sub>m</sub>/O<sub>2</sub> adsorption complexes, the three adsorption patterns, Pauling, Griffith and Yeager, are observed for Pt adsorption site with the complete list of structures reported in Fig. S11. No general trend is observed for the binding energy with respect to the cluster size. The spin density values remain high even after O<sub>2</sub> adsorption. Adsorption of O<sub>2</sub> upon pure Pt clusters is accompanied by high adsorption energy compared to that of pure Au clusters, which is quite expectable. Therefore, the most salient conclusion from Fig. 5 is that Au/Pt bimetallic clusters are energetically more active candidates for adsorption of O<sub>2</sub> than the corresponding pure metals. Substitution of a single Au atom with pure Pt<sub>m</sub> clusters results in a substantial improvement in oxygen adsorption. For instance, AuPt<sub>4</sub> exhibits a 57.7% increase in adsorption energy compared to that of the pure Pt<sub>5</sub> cluster (from -1.49 for Pt<sub>5</sub> to -2.35 eV for AuPt<sub>4</sub>). The same scenario appears for Au<sub>n-1</sub>Pt<sub>1</sub> clusters where the introduction of a single Pt atom to the pure Au<sub>n</sub> clusters is sufficient to drastically increase the strength of O<sub>2</sub> adsorption on Au<sub>n-1</sub>Pt<sub>1</sub> bimetallic clusters. Consider just Au<sub>3</sub>Pt with a 213.0% increase in adsorption energy compared to that of the pure Au<sub>4</sub> cluster (from -0.54 to -1.69 eV). Additionally, Au/Pt bimetallic clusters with higher Pt compositions show higher degree of adsorption (with one exception;  $E_{\text{ads}}(\text{Au}_3\text{Pt}_2) > E_{\text{ads}}(\text{Au}_2\text{Pt}_3)$ ). From the geometry viewpoint, a noticeable feature, being easily recognized is that O<sub>2</sub> adsorption predominantly occurs on the Pt site of Au/Pt bimetallic cluster if both Pt and Au sites are available. Griffith and Yeager are the best patterns for O<sub>2</sub> adsorption over Au/Pt bimetallic clusters. The O-O and M-O bond distances reported in Fig. 5 (including lowest minimum structures) and in Fig. S1, (including other low-lying minimum structures) indicate that all the studied Au<sub>m</sub>Pt<sub>n</sub> clusters have catalytic activity towards O<sub>2</sub> reduction. To facilitate an understanding of different factors in catalytic behavior of bimetallic clusters, Fig. 6 collects data from Fig. 5 and S11 and allow one to conclude that, regardless of the nature of the cluster (pure or alloyed) and the type of the site exposed to adsorption (Au or Pt), more than 90% (29 out of 32 low-lying minimum structures) of Pauling adsorption mode structures show an O-O bond elongation in the range of 1.27-1.29Å (4.1-7.4% elongation), and that in

more than 80% (17 out of 21 low-lying minimum structures) of the Griffith adsorption pattern structures, the O-O distance is extended to a range of 1.33-1.35 Å (9.9-11.6% increase) and, finally, that more than 86% (19 out of 22 low-lying minimum structures) of Yeager adsorption pattern structures have O-O bond distances which have increased to 1.36-1.42 Å range (12.4-17.4% elongation). This comparison clearly shows that catalytic activity of the studied clusters towards O-O bond weakening is highly dependent upon the “adsorption configuration” and is independent of the nature of the cluster (pure or alloyed) and of the site exposed to adsorption (Au or Pt). As expected, in all three cases, the number of “adsorption configurations” at which O<sub>2</sub> binds to Pt site is larger than those involving the Au adsorption site. Clearly, the catalytic activity of the clusters towards ORR is determined not only by the degree of O-O bond weakening/dissociation through adsorption, but also by the bond formation between the oxygen and the metallic cluster (M-O).

Next, we focus on the electronic structure of the oxygen adsorption complexes. Molecular oxygen has a triplet ground state with the unpaired electrons occupying the degenerate anti-bonding  $2\pi_u^*$  orbitals formed by the O (2p) atomic orbitals perpendicular to the molecular axis. Charge transfer from the metal cluster to the electrophilic O<sub>2</sub> molecule enhances the electron density in the O<sub>2</sub>  $2\pi_u^*$  orbital which consequently increases the O-O bond length. For all the lowest minimum structures, the amount of charge transfer measured from the calculated Bader charges is reported in Table 2, starred atoms refer to those which are directly connected to the O atom. At the first glance, one notices that all the metal atoms connected to the O atoms carry the positive charge and the net charge on the adsorbed O<sub>2</sub> molecule is, not surprisingly, always negative. In addition to the amounts of charge transferred between two fragments, “charge polarization” through metal cluster is quite significant. Apparently, the range of charge exchanged between metal cluster and adsorbed O<sub>2</sub> molecule is correlated to the different adsorption patterns. Almost all the Yeager structures (9 out of 10 structures) show a high degree of charge transfer between two fragments (0.57-0.67 e). The only exception is Au<sub>3</sub>/O<sub>2</sub> complex. The comparatively small charge transfer, 0.41e, for this complex is due to the large Au-O bond distance (2.21 Å) which destroys the effective interaction between two fragments and decreases the charge transferred accordingly. In Griffith adsorption configurations, O<sub>2</sub> receives less charge than that in Yeager structures, 0.34-0.49e, whereas in Pauling configurations one finds the smallest amount of charge transfer, regardless of cluster composition or metal identity (0.19-0.36 e). Interestingly, both O-O bond distance and charge transfer are highly correlated to the

adsorption configuration (Fig. 7) illustrating the dominant effect of charge transfer on O-O bond weakening.

*O<sub>2</sub> adsorption on pure Au (Pt) and CNT supported bimetallic AuPt clusters*

We are now in the position to examine the catalytic activity of supported Au<sub>m</sub>Pt<sub>n</sub> nanoparticles towards oxygen to shed light activation reactions. The lowest energy minimum structures obtained through a systematic search, involving a large number of initial geometries, are presented in Fig. 8. Other higher energy stable configurations are reported in Figure S12. Adsorption energy,  $E_{ads}$ , values in Fig. 8 are calculated as in eqn ( 6)

$$E_{ads} = E_{complex} - (E_{O_2} - E_{cluster/CNT}) \quad (6)$$

where  $E_{complex}$ ,  $E_{O_2}$  and  $E_{cluster/CNT}$  stand for the total energy of Au<sub>m</sub>Pt<sub>n</sub>-O<sub>2</sub>/CNT complex, O<sub>2</sub> molecule and Au<sub>m</sub>Pt<sub>n</sub>/CNT supported cluster, respectively. Fig. 8 shows that, in all cases involving two available adjacent Pt atoms, O<sub>2</sub> prefers to bind on the supported clusters via Yeager adsorption pattern whereas and in cases with only one available active site Pauling structure is strongly preferred. Note also that Griffith structure is not a favorable adsorption pattern for O<sub>2</sub> molecule leading to structures at energies higher than that of the ground state (Fig.S12). The O-O bond distance in Pauling structures varies in the range of 1.26-1.33 Å which shows some degree of bond elongation compared to that of the unsupported clusters (1.27-1.29 Å). For Yeager structures, however, the range of O-O bond length is almost the same (1.36-1.42 Å) for O<sub>2</sub> on supported or unsupported clusters. Another significant feature of Fig. 8 is the drastic decrease of O<sub>2</sub> adsorption energy on CNT-supported bimetallic clusters compared to that of the corresponding unsupported clusters reported in Fig. 5. This reduction is a direct consequence of change of coordination of the active adsorption sites due to the fact that, for the CNT supported clusters, some of the metal active sites (Au or Pt) are involved in metal-carbon bonds.

To ease the discussion, Fig. 9 presents M-O bond distances for adsorption complexes involving supported Au<sub>m</sub>Pt<sub>n</sub> clusters and shows that, not unexpectedly, they are similar to those involving the unsupported isolated clusters but with some noticeable differences as well. Moreover, this figure clearly shows a correlation between the M-O bond distances and between adsorption configuration and identity of the metal atom(s) bound to oxygen. Thus, the M-O bond distances for Pauling structures including supported bimetallic clusters and a Pt adsorption site are in the 1.95-2.05 Å range whereas for the corresponding isolated clusters the distances are shorter (1.87-1.97 Å). However, no significant difference is observed in corresponding values for isolated and CNT-supported clusters involving Au adsorption sites

which are always in the 2.05-2.23 Å range. The increasing trend of M-O bond distances in supported clusters, compared to those of isolated ones, also appears in the Yeager structures with M-O bond distances in the 1.94-2.03 Å range for the unsupported clusters to values in the 1.96-2.18 Å range for the supported ones and for both Pt and Au adsorption sites.

However, for the  $\text{Au}_m\text{-O}_2/\text{CNT}$  and  $\text{Pt}_m\text{-O}_2/\text{CNT}$  complexes, the trends in adsorption energy are rather irregular. In fact, while  $\text{O}_2$  adsorption energy of CNT-supported  $\text{Pt}_3$  and  $\text{Pt}_4$  is significantly reduced compared to the corresponding value for the isolated clusters, adsorption energy of  $\text{O}_2$  on  $\text{Pt}_2$  is increased from 1.31 eV for the isolated cluster to 2.01 eV for the supported one. The enhanced adsorption energy of  $\text{O}_2$  for  $\text{Pt}_2\text{-O}_2/\text{CNT}$  might be attributed to its particular Yeager configuration providing a favorable coordination environment and right orientation for an effective interaction with  $\text{O}_2$  molecule as well as with carbon surface. The low stability of supported adsorption complexes and their corresponding elongated O-O and M-O bond lengths are indicative of the weak binding interaction between the activated  $\text{O}_2$  molecule and the CNT-supported cluster. These structural changes facilitate further reaction steps towards  $\text{O}_2$  reduction, showing the significant role of the CNT support in facilitating the oxygen reduction reaction.

To better understand the trends described above, we analyze the electronic structure of  $\text{Au}_m\text{Pt}_n\text{-O}_2/\text{CNT}$  complexes by inspecting Bader charge, band structure and projected density of states. The simplest geometries for the  $\text{Au}_2\text{-O}_2/\text{CNT}$ ,  $\text{AuPt-O}_2/\text{CNT}$  and  $\text{Pt}_2\text{-O}_2/\text{CNT}$ , cases have been chosen as illustrative examples. Table 3 summarizes the Bader charges for supported clusters, without and with adsorbed  $\text{O}_2$ , and the net charge on the CNT before and after  $\text{O}_2$  adsorption. Similar to previous tables, the positive and the negative values represent the losing and gaining charge, respectively, and the starred atoms refer to those which are directly bound to the surface. The analysis of Table 3 shows that metal atoms directly connected to the CNT surface are always positively charged whereas those farther away are negatively charged. These negatively charged active sites are the best candidates to interact with electrophilic species like the  $\text{O}_2$  molecule becoming significantly positively charge upon  $\text{O}_2$  adsorption although metal atoms connected to the carbon surface still remain positively charged. The localized negative charge on O atoms confirms the charge transfer from the CNT supported clusters to the adsorbed  $\text{O}_2$  species. Moreover, there seems to be a linear dependence between the  $\text{O}_2$  elongation and the amount of the charge transfer; the minimum charge transfer (0.19 e) corresponds to a Pauling configuration of the  $\text{Au}_2\text{-O}_2/\text{CNT}$  complex which also shows the smallest O-O elongation (4.1%). On the other hand, the

maximum charge transfer (0.71 e) corresponds to the Yeager configuration of the O<sub>2</sub>Pt<sub>2</sub>/CNT complex with a concomitant maximum of O-O bond elongation (15.7%).

For the simplest Au<sub>2</sub>-O<sub>2</sub>/CNT, AuPt-O<sub>2</sub>/CNT and Pt<sub>2</sub>-O<sub>2</sub>/CNT adsorption complexes, Fig. 10 reports the density of states projected on Au, Pt and O<sub>2</sub>. For comparison, the PDOS of the corresponding non-interacting systems (O<sub>2</sub> and supported clusters are at infinite distance) is also included. In each non-interacting case, the electronic states located slightly below the Fermi state are the O<sub>2</sub> 2π\* anti-bonding, whereas those at -5 and -6.5 eV are the O<sub>2</sub> 2π and 5σ bonding states, respectively. In all cases, metal 5d states are placed between the 2π and 2π\* of the O<sub>2</sub> molecule. This electronic distribution, facilitates electron transfer between the metal 5d orbitals and O<sub>2</sub> 2π\* orbitals of molecule; which is in line with the direction of charge transfer from the supported cluster to the O<sub>2</sub> molecule.

Comparing the density of states before and after O<sub>2</sub> adsorption shows a noticeable modification in projected DOS of the interacting fragments (O<sub>2</sub> and supported clusters) near Fermi level. In some cases, such as Pt<sub>2</sub>-O<sub>2</sub>/CNT, d band becomes delocalized, broadened, and largely modified and a strong hybridization between these modified d states and 2π and 2π\* orbitals of O<sub>2</sub> occurs through almost the entire energy region. As expected, deformation of DOS for Au<sub>2</sub>-O<sub>2</sub>/CNT is not as pronounced as Pt<sub>2</sub>-O<sub>2</sub>/CNT. The narrow and sharp bands of the isolated (non-interacting case) O<sub>2</sub> molecule become somehow broadened and delocalized when it adsorbed through a weak overlap between Au 6s and 5d orbitals and O<sub>2</sub> 2π orbitals.

## Conclusions

Motivated by the experimentally observed higher catalytic activity of supported AuPt binary alloys towards oxygen reduction reactions, a systematic study of the interaction of oxygen with unsupported and CNT-supported Au<sub>m</sub>Pt<sub>n</sub> (2 ≤ m+n ≤ 4) nanoparticles has been carried out in the framework of density functional theory. This involves searching for the lowest energy structures of the pure Au<sub>m</sub>, Pt<sub>n</sub>, and Au<sub>m</sub>Pt<sub>n</sub> bimetallic clusters (2 ≤ m+n ≤ 5), investigating the improved behavior of alloyed clusters compared to the pure ones, finding the most stable configurations of Au<sub>m</sub>, Pt<sub>n</sub> and Au<sub>m</sub>Pt<sub>n</sub> clusters (2 ≤ m+n ≤ 4) supported on single-walled (5-5)-carbon nanotube and determining their electronic and geometric features and, finally, investigating O<sub>2</sub> adsorption molecule on unsupported and CNT-supported. The main results of our investigations are summarized as follows.

- For a given cluster size, bimetallic PtAu clusters with higher content of Pt clusters are thermodynamically more stable. Analysis of the electronic structure indicates that improved activity of the PtAu binary alloy clusters compared to the pure Pt or Au clusters can be

attributed to the particular distribution of the electronic charge which increases the ability of these centers for having a proper interaction with electrophilic species.

- For the supported PtAu binary clusters, Au atoms tend to be located towards the vacuum, and adsorption occurs always via Pt head or Pt-Pt edge. Electronic analysis of binary structures confirms the presence of the substantial density of states at the vicinity of Fermi level dominated by Pt 5d orbitals which agrees with the general trend of Pt interacting stronger than Au with the support C atoms.

- There is a positive correlation between the numbers of Pt atoms in cluster and adsorption energy. There also exists a positive correlation between the strength of binding to the substrate and the extent of charge transfer.

- PtAu bimetallic clusters are energetically more active for O<sub>2</sub> adsorption than the corresponding pure monometallic clusters with O<sub>2</sub> adsorption, predominantly occurring on the Pt site if both Pt and Au sites are available. Adsorption configuration and identity of the site exposed to adsorption are the two main factors controlling the catalytic activity of the clusters. Charge distribution analysis shows a strong linear correlation between the O-O bond elongation and the amount of the charge transferred to O<sub>2</sub> molecule.

- The present model calculations indicate that the catalytic activity of the PtAu clusters towards oxygen reduction is improved when they are supported on CNT. Interestingly, this is associated with a drastic decrease of thermodynamic stability of the complexes compared to that of the corresponding unsupported clusters.

- The charge transfer from CNT appears to have the dominant effect on catalytic ability of the supported bimetallic clusters. The calculated density of states projected on Au, Pt and O<sub>2</sub>, before and after adsorption, shows a significant modification upon O<sub>2</sub> adsorption, which can provide a reasonable explanation for adsorption behavior of the systems.

Undoubtedly, the conclusions above have been extracted from a series of models systems and the theoretical predictions require experimental verification. Nevertheless, the main conclusions described above pave the way for further studies regarding O<sub>2</sub> reduction and are expected to help scientists to open up new avenues for tailoring more efficient and active catalysts with improved properties.



**Acknowledgements**

F. N. is grateful to the Institute for Advanced Studies in Basic Sciences, for financial support. The research of F. I. has been supported by Spanish MICINN through research grant CTQ2012-30751, Generalitat de Catalunya grants 2014SGR97 and XRQTC and through the 2009 ICREA Academia Award for Excellence in University Research.

**Table 1:** Bader charges (a.u.) on metal cluster atoms.  $\Delta q$  stands for the Bader charge on the CNT. Positive/negative values indicate the charge depletion and accumulation upon adsorption. The starred atoms are those which directly bind to the surface.

	$E_{\text{ads}}$ (eV)	$\Delta q$	Partial charge on each atom			
Au <sub>4</sub> /CNT	-0.57	0.04	$q_{\text{Au1}}^*$ 0.22	$q_{\text{Au2}}$ -0.07	$q_{\text{Au3}}$ -0.16	$q_{\text{Au4}}$ -0.03
Au <sub>3</sub> Pt/CNT	-2.22	0.08	$q_{\text{Au1}}$ 0.01	$q_{\text{Au2}}$ -0.14	$q_{\text{Au3}}$ -0.14	$q_{\text{Pt4}}^*$ 0.20
Au <sub>2</sub> Pt <sub>2</sub> /CNT	-2.73	-0.09	$q_{\text{Pt1}}^*$ 0.14	$q_{\text{Au2}}$ -0.10	$q_{\text{Pt3}}^*$ 0.16	$q_{\text{Au4}}$ -0.11
AuPt <sub>3</sub> /CNT	-3.17	-0.07	$q_{\text{Pt1}}^*$ 0.20	$q_{\text{Pt2}}^*$ 0.10	$q_{\text{Pt3}}$ -0.11	$q_{\text{Au4}}$ -0.13
Pt <sub>4</sub> /CNT	-3.37	-0.18	$q_{\text{Pt1}}^*$ 0.12	$q_{\text{Pt2}}$ 0.13	$q_{\text{Pt3}}$ -0.20	$q_{\text{Pt4}}^*$ 0.12
Au <sub>3</sub> /CNT	-1.04	-0.09	$q_{\text{Au1}}$ 0.11	$q_{\text{Au2}}$ -0.10	$q_{\text{Au3}}$ 0.08	
Au <sub>2</sub> Pt/CNT	-1.96	0.04	$q_{\text{Pt1}}^*$ 0.13	$q_{\text{Au2}}$ -0.09	$q_{\text{Au3}}$ -0.08	
AuPt <sub>2</sub> /CNT	-3.24	-0.08	$q_{\text{Pt1}}^*$ 0.13	$q_{\text{Pt2}}^*$ 0.15	$q_{\text{Au3}}$ -0.20	
Pt <sub>3</sub> /CNT	-3.21	-0.06	$q_{\text{Pt1}}^*$ 0.14	$q_{\text{Pt2}}$ -0.23	$q_{\text{Pt3}}^*$ 0.15	
Au <sub>2</sub> /CNT	-0.90	0.07	$q_{\text{Au1}}^*$ 0.15	$q_{\text{Au2}}$ -0.22		
AuPt/CNT	-2.35	0.11	$q_{\text{Au1}}$ -0.26	$q_{\text{Pt2}}^*$ 0.15		
Pt <sub>2</sub> /CNT	-2.34	-0.08	$q_{\text{Pt1}}^*$ 0.04	$q_{\text{Pt2}}^*$ 0.04		

**Table 2.** Bader charges (a.u.) for Au<sub>m</sub>Pt<sub>n</sub>/O<sub>2</sub> adsorption complexes. The positive and negative values indicate the loosing and gaining the charge upon adsorption. The starred atoms are those which directly bind to O<sub>2</sub> molecule.

Cluster	Charge on individual metal atom					Charge on O <sub>2</sub>	Adsorption Pattern
	Au(1)	Au(2) <sup>*</sup>	Au(3)	Au(4) <sup>*</sup>	Au(5)		
Au <sub>5</sub> O <sub>2</sub>	0.10	0.28	-0.06	0.28	-0.06	-0.54	Yeager
Au <sub>4</sub> PtO <sub>2</sub>	Au(1)	Au(2)	Au(3)	Au(4) <sup>*</sup>	Pt(5) <sup>*</sup>	-0.61	Yeager
	-0.07	0.08	-0.10	0.36	0.35		
Au <sub>3</sub> Pt <sub>2</sub> O <sub>2</sub>	Au(1)	Au(2)	Au(3)	Pt(4) <sup>*</sup>	Pt(5) <sup>*</sup>	-0.62	Yeager
	0.08	-0.11	-0.11	0.39	0.38		
Au <sub>2</sub> Pt <sub>3</sub> O <sub>2</sub>	Pt(1) <sup>*</sup>	Pt(2)	Au(3)	Au(4)	Pt(5) <sup>*</sup>	-0.64	Yeager
	0.41	0.07	-0.13	-0.12	0.42		
AuPt <sub>4</sub> O <sub>2</sub>	Pt(1)	Pt(2) <sup>*</sup>	Pt(3) <sup>*</sup>	Pt(4)	Au(5)	-0.60	Yeager
	-0.13	0.42	0.36	0.04	-0.09		
Pt <sub>5</sub> O <sub>2</sub>	Pt(1)	Pt(2)	Pt(3) <sup>*</sup>	Pt(4) <sup>*</sup>	Pt(5)	-0.67	Yeager
	0.044	0.05	0.36	0.31	-0.10		
Au <sub>4</sub> O <sub>2</sub>	Au(1) <sup>*</sup>	Au(2)	Au(3)	Au(4)		-0.21	Pauling
	0.31	-0.01	-0.16	0.06			
Au <sub>3</sub> PtO <sub>2</sub>	Au(1)	Au(2)	Au(3)	Pt(4) <sup>*</sup>		-0.41	Griffith
	0.05	-0.07	-0.07	0.51			
Au <sub>2</sub> Pt <sub>2</sub> O <sub>2</sub>	Au(1)	Au(2)	Pt(3) <sup>*</sup>	Pt(4)		-0.49	Griffith
	-0.041	-0.017	0.51	0.039			
AuPt <sub>3</sub> O <sub>2</sub>	Pt(1) <sup>*</sup>	Pt(2)	Pt(3) <sup>*</sup>	Au(4)		-0.60	Yeager
	0.42	-0.12	0.37	-0.07			
Pt <sub>4</sub> O <sub>2</sub>	Pt(1) <sup>*</sup>	Pt(2)	Pt(3)	Pt(4) <sup>*</sup>		-0.65	Yeager
	0.36	-0.07	0.01	0.35			
Au <sub>3</sub> O <sub>2</sub>	Au(1) <sup>*</sup>	Au(2)	Au(3) <sup>*</sup>			-0.41	Yeager
	0.21	0.00	0.20				
Au <sub>2</sub> PtO <sub>2</sub>	Pt(1) <sup>*</sup>	Au(2)	Au(3)			-0.43	Griffith
	0.45	-0.01	-0.01				
AuPt <sub>2</sub> O <sub>2</sub>	Pt(1) <sup>*</sup>	Pt(2) <sup>*</sup>	Au(3)			-0.57	Yeager
	0.34	0.35	-0.13				
Pt <sub>3</sub> O <sub>2</sub>	Pt(1) <sup>*</sup>	Pt(2)	Pt(3)			-0.47	Griffith
	0.47	-0.00	0.01				
Au <sub>2</sub> O <sub>2</sub>	Au(1)	Au(1) <sup>*</sup>				-0.19	Pauling
	-0.06	0.25					
AuPtO <sub>2</sub>	Au(1)	Pt(2) <sup>*</sup>				-0.34	Griffith
	-0.11	0.45					
Pt <sub>2</sub> O <sub>2</sub>	Pt(1)	Pt(2) <sup>*</sup>				-0.40	Griffith
	-0.08	0.48					

**Table 3.** Bader charges (a.u.) for  $Au_mPt_n-O_2/CNT$  adsorption complexes. The net charge on CNT before and after  $O_2$  adsorption is included for comparison. The starred atoms are those which directly bind to the surface of nanotube.

System	q (on each metal atom and $O_2$ )					$\Delta q_{CNT}$ (after $O_2$ ads.)	$\Delta q_{CNT}$ (before $O_2$ ads.)
	Au(1) <sup>*</sup>	Au(2)	Au(3)	Au(4)	Ads. $O_2$		
$Au_4-O_2/CNT$	Au(1) <sup>*</sup>	Au(2)	Au(3)	Au(4)	Ads. $O_2$	0.12	0.04
	0.15	0.15	-0.09	0.32	-0.65		
$Au_3Pt-O_2/CNT$	Au(1)	Au(2)	Au(3)	Pt(4) <sup>*</sup>	Ads. $O_2$	0.13	0.07
	-0.12	-0.01	0.17	0.18	-0.35		
$Au_2Pt_2-O_2/CNT$	Pt(1) <sup>*</sup>	Au(2)	Pt(3) <sup>*</sup>	Au(4)	Ads. $O_2$	-0.05	-0.09
	0.16	0.30	0.40	-0.11	-0.70		
$AuPt_3-O_2/CNT$	Pt(1) <sup>*</sup>	Pt(2) <sup>*</sup>	Pt(3)	Au(4)	Ads. $O_2$	-0.04	-0.07
	0.42	0.16	0.31	-0.17	-0.67		
$Pt_4-O_2/CNT$	Pt(1) <sup>*</sup>	Pt(2) <sup>*</sup>	Pt(3)	Pt(4) <sup>*</sup>	Ads. $O_2$	-0.11	-0.18
	0.11	0.09	0.19	0.38	-0.66		
$Au_3-O_2/CNT$	Au(1) <sup>*</sup>	Au(2)	Au(3) <sup>*</sup>		Ads. $O_2$	0.0472	-0.0888
	0.20	-0.07	0.26		-0.44		
$Au_2Pt-O_2/CNT$	Pt(1) <sup>*</sup>	Au(2)	Au(3)		Ads. $O_2$	0.06	0.04
	0.16	0.23	-0.08		-0.38		
$AuPt_2-O_2/CNT$	Pt(1) <sup>*</sup>	Pt(2) <sup>*</sup>	Au(3)		Ads. $O_2$	-0.013	-0.08
	0.13	0.13	0.08		-0.33		
$Pt_3-O_2/CNT$	Pt(1) <sup>*</sup>	Pt(2)	Pt(3) <sup>*</sup>		Ads. $O_2$	-0.0575	-0.0577
	0.05	0.22	0.47		-0.68		
$Au_2-O_2/CNT$	Au(1) <sup>*</sup>	Au(2)			Ads. $O_2$	-0.09	0.07
	0.06	0.04			-0.19		
$AuPt-O_2/CNT$	Au(1)	Pt(2) <sup>*</sup>			Ads. $O_2$	0.13	0.11
	0.06	0.11			-0.29		
$Pt_2-O_2/CNT$	Pt(1) <sup>*</sup>	Pt(2) <sup>*</sup>			Ads. $O_2$	-0.08	-0.08
	0.40	0.38			-0.71		

### Captions for Figures

**Figure 1.** The four effective adsorption sites on an armchair CNT.

**Figure 2.** Energetically most stable adsorption conformers of  $Au_mPt_n/CNT$

**Figure 3.** Summary of metal-carbon (M-C) distances for the different adsorption sites: top (T) and bridge ( $B_{axial}$  and  $B_{zigzag}$ ).

**Figure 4.** Projected density of states and electronic band structures for bare CNT,  $Au_2/CNT$ ,  $Pt_2/CNT$  and  $AuPt/CNT$  adsorption complexes. The zero of the energy corresponds to the Fermi level.

**Figure 5.** Computed adsorption energy (eV), magnetic moment, and relevant bond lengths for the most stable geometries of  $Au_mPt_n/O_2$  with  $2 \leq m+n \leq 5$ .

**Figure 6.** Distribution of O-O bond distances *versus*  $O_2$  adsorption energy. Blue and red squares represent the Pauling adsorption patterns with Pt and Au adsorption centers, respectively. Green and orange squares correspond to the Griffith and Yeager adsorption patterns, respectively.

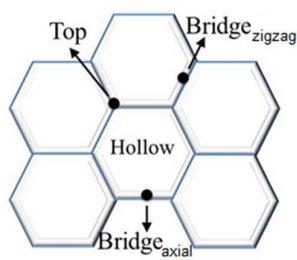
**Figure 7.** O-O bond distance as a function of charge transfer from cluster to  $O_2$  molecule.

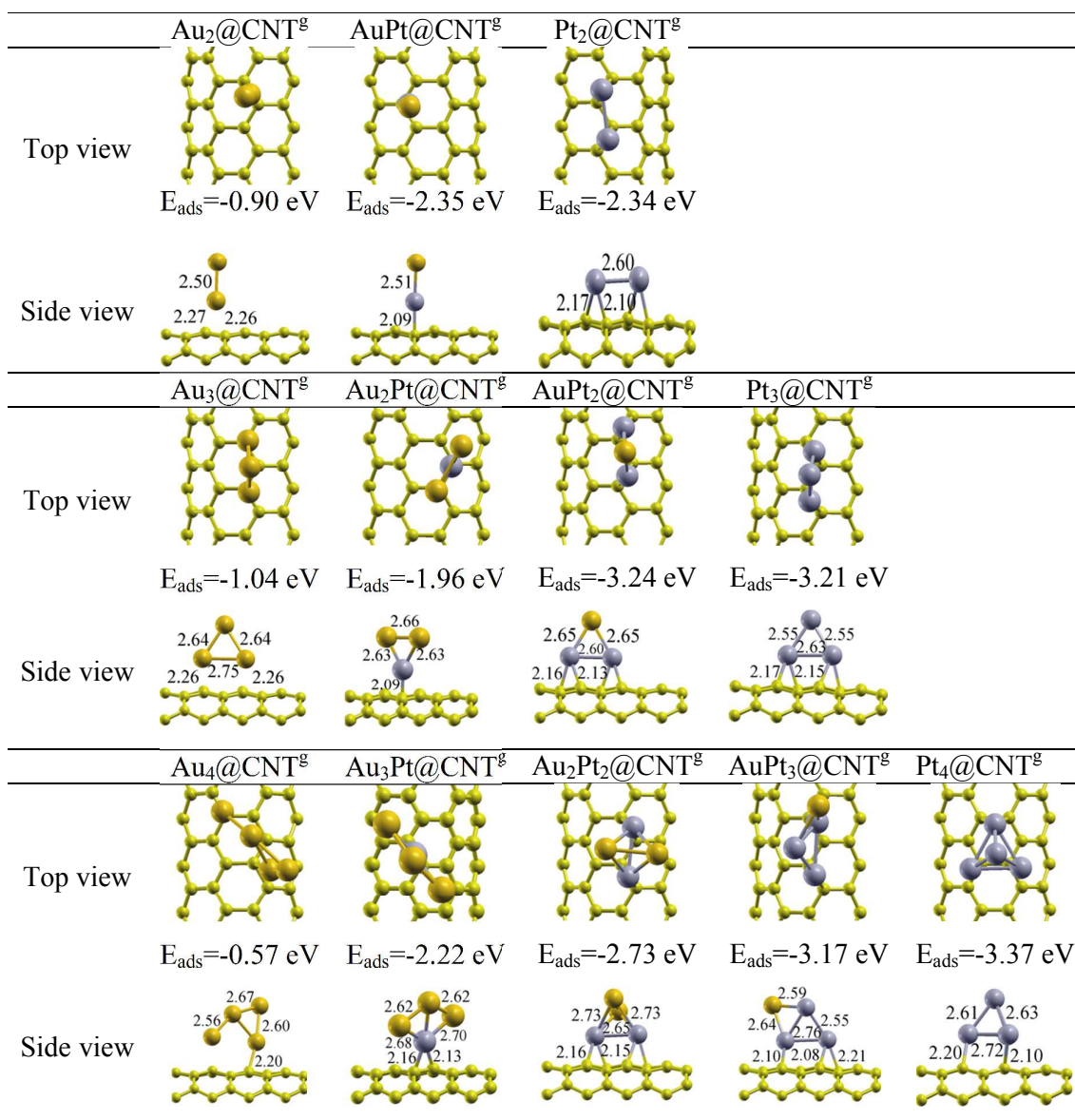
**Figure 8.** The lowest energy structures of  $O_2$  adsorbed on CNT-supported  $Au_mPt_n$  clusters ( $2 \leq m+n \leq 4$ ), corresponding adsorption energies ( $E_{ads}$ , eV), spin densities ( $\mu$ , Bohr magneton) and bond distances ( $\text{\AA}$ ) of O-O and metal-O (M-O) after adsorption.

**Figure 9** Metal-O bond distances ( $\text{\AA}$  units) of adsorption complexes  $Au_mPt_n-O_2/CNT$  for different adsorption patterns Pauling (P), Griffith (G), Yeager (Y) and the identity of the metal (Au and Pt) exposed to adsorption.

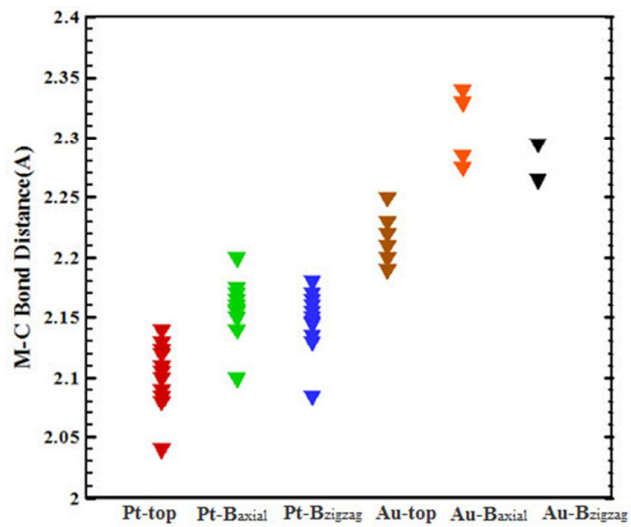
**Figure 10.** Plots of density of states projected on s, p and d orbitals of C, Pt and Au in complexes  $Au_2-O_2/CNT$ ,  $AuPt-O_2/CNT$  and  $Pt_2-O_2/CNT$ . DOS for interacting and non-interacting systems ( $O_2$  and supported clusters are positioned in an infinite separation distance) are compared.

**Figure 1.** The four effective adsorption sites on an armchair CNT.



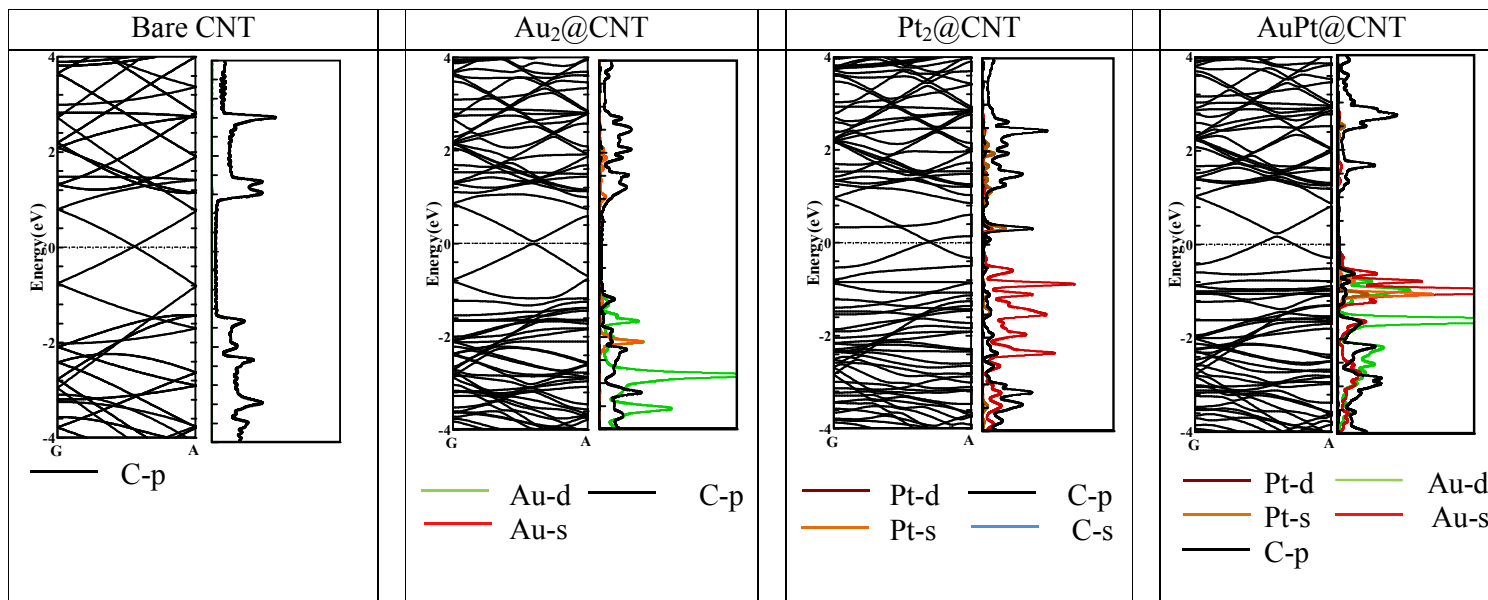
**Figure 2.** Energetically most stable adsorption conformers of  $Au_mPt_n/CNT^g$ 

**Figure 3.** Summary of metal-carbon (M-C) distances for the different adsorption sites: top (T) and bridge ( $B_{axial}$  and  $B_{zigzag}$ ).

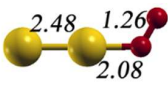
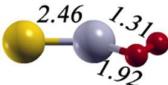
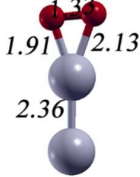
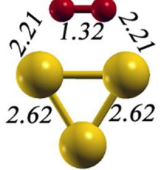
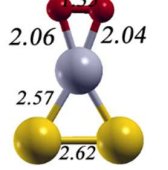
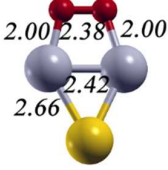
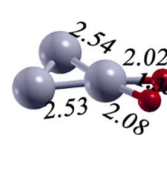
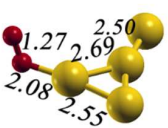
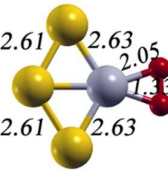
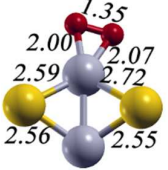
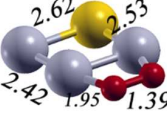
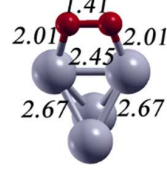
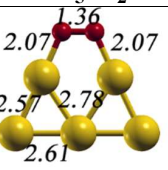
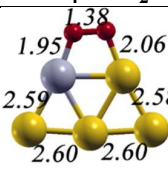
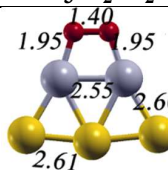
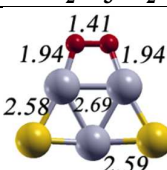
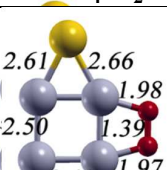
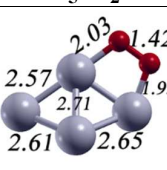




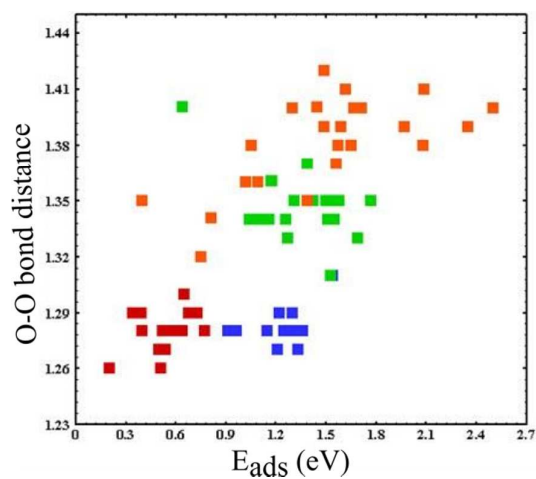
**Figure 4.** Projected density of states and electronic band structures for bare CNT, Au<sub>2</sub>/CNT, Pt<sub>2</sub>/CNT and AuPt/CNT adsorption complexes. The zero of the energy corresponds to the Fermi level.

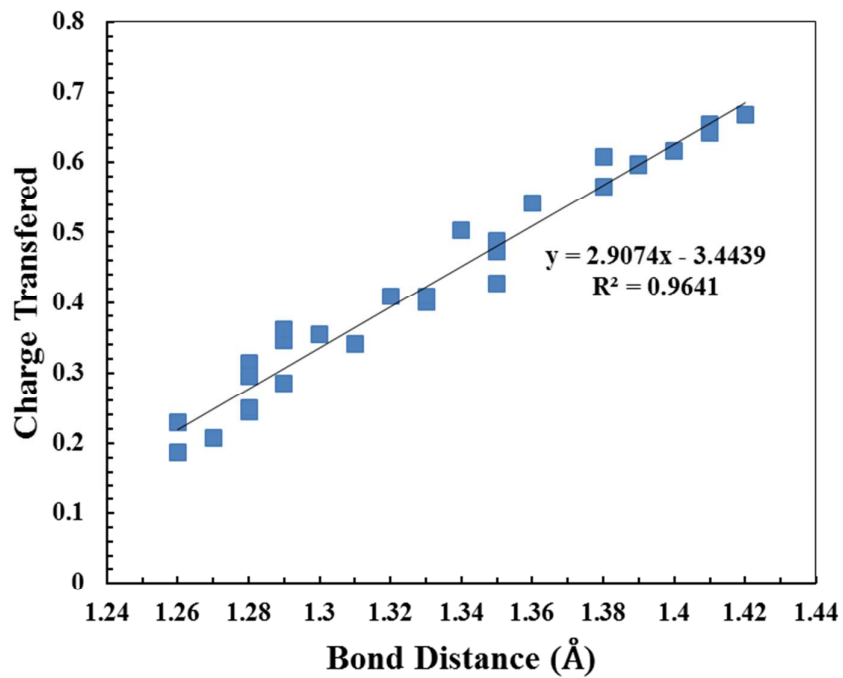


**Figure 5.** Computed adsorption energy (eV), magnetic moment, and relevant bond lengths for the most stable geometries of  $\text{Au}_m\text{Pt}_n/\text{O}_2$  with  $2 \leq m+n \leq 5$ .

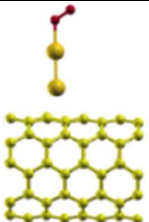
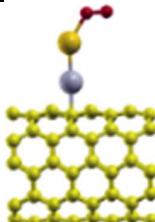
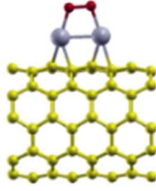
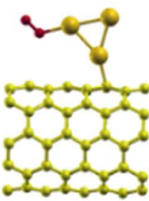
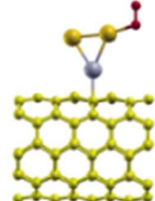
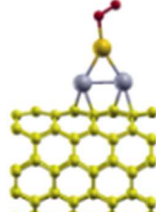
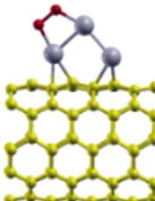
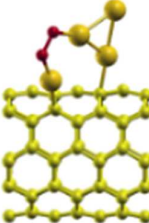
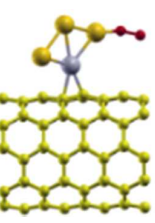
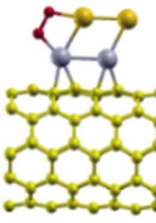
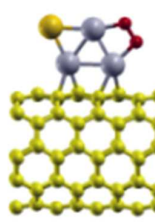
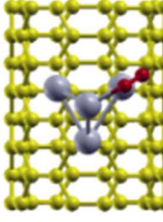
	<b><math>\text{Au}_2/\text{O}_2</math></b>	<b><math>\text{AuPt}/\text{O}_2</math></b>	<b><math>\text{Pt}_2/\text{O}_2</math></b>			
						
$E_{\text{ads}}$	-0.51	-1.54	-1.31			
$\mu$	2	1	2			
O-O	1.26	1.31	1.33			
M-O	2.08	1.92	1.91-2.13			
	<b><math>\text{Au}_3/\text{O}_2</math></b>	<b><math>\text{Au}_2\text{Pt}/\text{O}_2</math></b>	<b><math>\text{AuPt}_2/\text{O}_2</math></b>	<b><math>\text{Pt}_3/\text{O}_2</math></b>		
						
$E_{\text{ads}}$	-0.75	-1.53	-2.08	-1.58		
$\mu$	1	2	1	2		
O-O	1.32	1.35	2.38	1.35		
M-O	2.21-2.21	2.06-2.04	2.00-2.00	2.02-2.08		
	<b><math>\text{Au}_4/\text{O}_2</math></b>	<b><math>\text{Au}_3\text{Pt}/\text{O}_2</math></b>	<b><math>\text{Au}_2\text{Pt}_2/\text{O}_2</math></b>	<b><math>\text{AuPt}_3/\text{O}_2</math></b>	<b><math>\text{Pt}_4/\text{O}_2</math></b>	
						
$E_{\text{ads}}$	-0.54	-1.69	-1.55	-1.97	-1.62	
$\mu$	2	1	2	1	2	
O-O	1.27	1.33	1.35	1.39	1.41	
M-O	2.08	2.05-2.05	2.00-2.07	1.95-1.69	2.01-2.01	
	<b><math>\text{Au}_5/\text{O}_2</math></b>	<b><math>\text{Au}_4\text{Pt}/\text{O}_2</math></b>	<b><math>\text{Au}_3\text{Pt}_2/\text{O}_2</math></b>	<b><math>\text{Au}_2\text{Pt}_3/\text{O}_2</math></b>	<b><math>\text{AuPt}_4/\text{O}_2</math></b>	<b><math>\text{Pt}_5/\text{O}_2</math></b>
						
$E_{\text{ads}}$	-1.18	-1.57	-2.50	-2.09	-2.35	-1.49
$\mu$	1	2	1	2	1	4
O-O	1.36	1.38	1.40	1.41	1.39	1.42
M-O	2.07-2.07	1.95-2.06	1.95-1.95	1.94-1.94	1.98-1.97	2.03-1.95

**Figure 6.** Distribution of O-O bond distances *versus* O<sub>2</sub> adsorption energy. Blue and red squares represent the Pauling adsorption patterns with Pt and Au adsorption centers, respectively. Green and orange squares correspond to the Griffith and Yeager adsorption patterns, respectively.



**Figure 7.** O-O bond distance as a function of charge transfer from cluster to O<sub>2</sub> molecule.

**Figure 8.** The lowest energy structures of O<sub>2</sub> adsorbed on CNT-supported Au<sub>m</sub>Pt<sub>n</sub> clusters (2 ≤ m+n ≤ 4), corresponding adsorption energies (E<sub>ads</sub>, eV), spin densities (μ, Bohr magneton) and bond distances (Å) of O-O and metal-O (M-O) after adsorption.

	<b>Au<sub>2</sub>-O<sub>2</sub> /CNT</b>	<b>AuPt-O<sub>2</sub> /CNT</b>	<b>Pt<sub>2</sub>-O<sub>2</sub> /CNT</b>		
					
E <sub>ads</sub>	-0.13	-0.15	-2.01		
μ	1.98	1.31	0.05		
O-O	1.26	1.28	1.40		
M-O	2.16	2.12	2.02-2.03		
	<b>Au<sub>3</sub>-O<sub>2</sub> /CNT</b>	<b>Au<sub>2</sub>Pt-O<sub>2</sub> /CNT</b>	<b>AuPt<sub>2</sub>-O<sub>2</sub> /CNT</b>	<b>Pt<sub>3</sub>-O<sub>2</sub> /CNT</b>	
					
E <sub>ads</sub>	-0.90	-0.70	-0.33	-1.06	
μ	1.11	1.20	1.41	0.00	
O-O	1.32	1.30	1.29	1.40	
M-O	2.06	2.09	2.15	1.98	
	<b>Au<sub>4</sub>-O<sub>2</sub> /CNT</b>	<b>Au<sub>3</sub>Pt-O<sub>2</sub> /CNT</b>	<b>Au<sub>2</sub>Pt<sub>2</sub>-O<sub>2</sub> /CNT</b>	<b>AuPt<sub>3</sub>-O<sub>2</sub> /CNT</b>	<b>Pt<sub>4</sub>-O<sub>2</sub> /CNT</b>
					
E <sub>ads</sub>	-0.97	-0.46	-1.37	-1.82	(top view) -1.09
μ	0.56	1.21	0.00	0.00	0.01
O-O	1.39	1.29	1.41	1.41	1.39
M-O	2.06-2.07	2.09	2.03-2.04	1.96-2.02	1.99-2.08

**Figure 9** Metal-O bond distances ( $\text{\AA}$  units) of adsorption complexes  $\text{Au}_m\text{Pt}_n\text{-O}_2/\text{CNT}$  for different adsorption patterns Pauling (P), Griffith (G), Yeager (Y) and the identity of the metal (Au and Pt) exposed to adsorption.

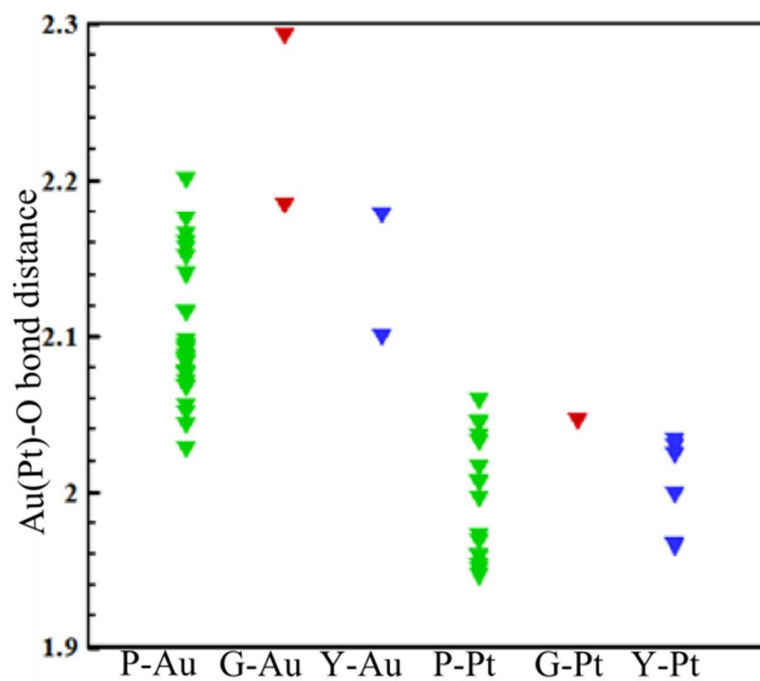
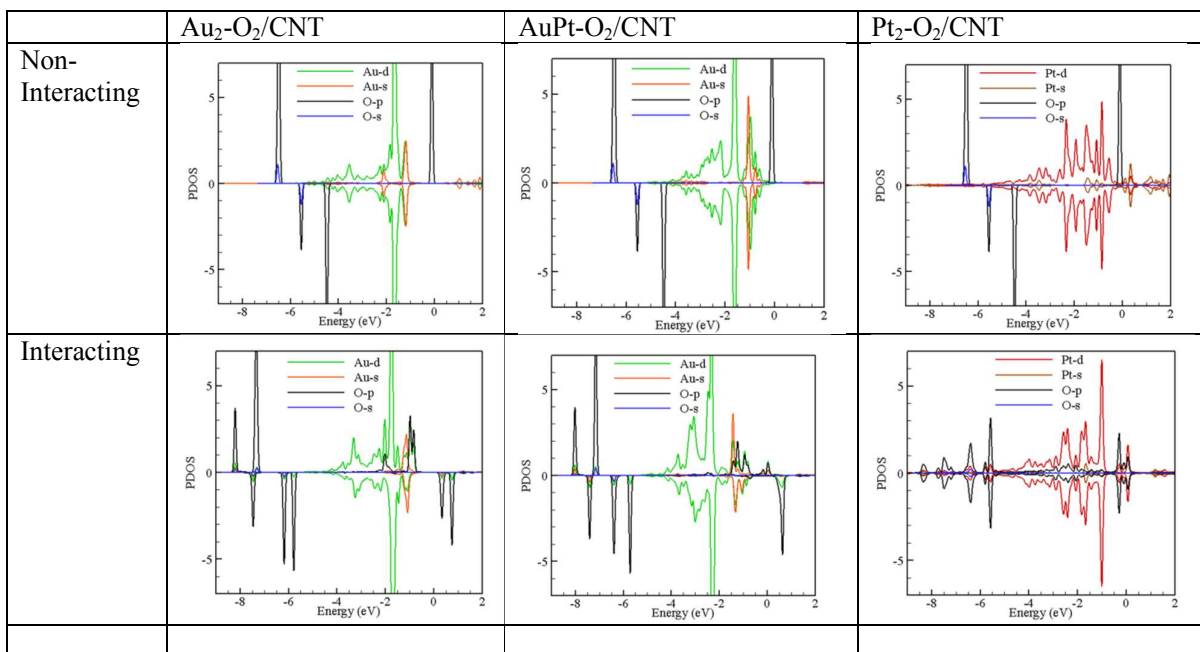


**Figure 10.** Plots of density of states projected on s, p and d orbitals of C, Pt and Au in complexes  $\text{Au}_2\text{-O}_2/\text{CNT}$ ,  $\text{AuPt-O}_2/\text{CNT}$  and  $\text{Pt}_2\text{-O}_2/\text{CNT}$ . DOS for interacting and non-interacting systems ( $\text{O}_2$  and supported clusters are positioned in an infinite separation distance) are compared



## References

---

- 1 L. Carrette, K. A. Friedrich and U. Stimming, *Chem. Phys. Chem.*, 2000, **1**, 162.
- 2 H. P. Dhar, *J. Electroanal. Chem.*, 1993, **357**, 237.
- 3 P. Costamagna and S. Srinivasan., *J. Power Sources*, 2001, **102**, 242.
- 4 G. Girishkumar, T. D. Hall, K. Vinodgopal and P. V. Kamat, *J. Phys. Chem. B*, 2006,**110**, 107.
- 5 Y. Lin, X. Cui, C. H. Yen and C. M. Wai, *Langmuir*, 2005, **21**, 11474.
- 6 T. L. Pham, P. V. Dung, A. Sugiyama, N. D. Duc, T. Shimoda, A. Fujiwara and D. H. Chi, *Comput. Mater. Sci.*, 2010, **49**, S15-S20.
- 7 C. Lamy, A. Lima, V. LeRhun, F. Delime, C. Coutanceau and J.-M. Leger, *J. Power Sources*, 2002, **105**, 283.
- 8 T. Iwasita, *Electrochim. Acta*, 2002, **47**, 3663.
- 9 F. Kadirgan, S. Beyhan and T. Atilan, *Int. J. Hydrogen Energy*, 2009, **34**, 4312. .
- 10 A. B. Anderson, *Electrochim. Acta*, 2002,**47**, 3759.
- 11 B. Grgur, N. Markovic and P. Ross, *Can. J. Chem.*, 1997, **75**, 1465.
- 12 V. Stamenkovic, N. M Markovic and P. Ross Jr., *J. Electroanal. Chem.*, 2001, **500**, 44.
- 13 N. Markovic, H. Gasteiger, B. Grgur and P. Ross, *J. Electroanal. Chem.*, 1999, **467**, 157.
- 14 P. Mani, R. Srivastava and P. Strasser, *J. Phys. Chem. C*, 2008, **112**, 2770.
- 15 S. Koh and P. Strasser, *J. Amer. Chem. Soc.*, 2007, **129**, 12624.
- 16 V. R. Stamenkovic, B. Fowler, B. S. Mun, G. Wang, P. N. Ross, C. A. Lucas and N. M. Markovic, *Science*, 2007, **315**, 493.
- 17 J. Zhang and J. Fang, *J. Amer. Chem. Soc.*, 2009, **131**, 18543.
- 18 C. Venkateswara Rao and B. Viswanathan, *J. Phys. Chem. C*, 2009, **113**, 18907.
- 19 Y. Kang and C. B. Murray, *J. Amer. Chem. Soc.*, 2010, **132**, 7568.
- 20 J. Kim, Y. Lee and S. Sun, *J. Amer. Chem. Soc.*, 2010, **132**, 4996.
- 21 V. Mazumder, M. Chi, K. L. More and S. Sun, *J. Amer. Chem. Soc.*, 2010, **132**, 7848.
- 22 C. Wang, D. van der Vliet, K.-C. Chang, H. You, D. Strmcnik, J. A. Schlueter, N. M. Markovic and V. R. Stamenkovic, *J. Phys. Chem. C*, 2009, **113**, 19365.
- 23 K. Jayasayee, V. A. Dam, T. Verhoeven, S. Celebi and F. A. de Bruijn, *J. Phys. Chem. C*, 2009, **113**, 20371.
- 24 T.-Y. Jeon, S. J. Yoo, Y.-H. Cho, K.-S. Lee, S. H. Kang and Y.-E. Sung, *J. Phys. Chem. C*, 2009,**113**, 19732.



- 
- 25 J. Wu, J. Zhang, Z. Peng, S. Yang, F. T. Wagner and H. Yang, *J. Amer. Chem. Soc.*, 2010, **132**, 4984.
- 26 A. Sarkar and A. Manthiram, *J. Phys. Chem. C*, 2010, **114**, 4725.
- 27 P. B. Balbuena, S. R. Calvo, E. J. Lamas, P. F. Salazar and J. M. Seminario, *J. Phys. Chem. B*, 2006, **110**, 17452.
- 28 P. B. Balbuena, D. Altomare, N. Vadlamani, S. Bingi, L. A. Agapito and J. M. Seminario *J. Phys. Chem. A*, 2004, **108**, 6378.
- 29 P. Balbuena, D. Altomare, L. Agapito and J. Seminario, *J. Phys. Chem. B*, 2003, **107**, 13671.
- 30 T. Li and P. B. Balbuena, *Chem. Phys. Lett.*, 2003, **367**, 439.
- 31 U. Paulus, A. Wokaun, G. Scherer, T. Schmidt, V. Stamenkovic, V. Radmilovic, N. Markovic and P. Ross, *J. Phys. Chem. B*, 2002, **106**, 4181.
- 32 V. S. Murthi, R. C. Urian and S. Mukerjee, *J. Phys. Chem. B*, 2004, **108**, 11011.
- 33 J. Zhang, Y. Mo, M. Vukmirovic, R. Klie, K. Sasaki and R. Adzic, *J. Phys. Chem. B*, 2004, **108**, 10955.
- 34 H. Zhang, Y. Yin, Y. Hu, C. Li, P. Wu, S. Wei and C. Cai, *J. Phys. Chem. C*, 2010, **114**, 11861.
- 35 H.-F. Yang, P.-y. Xie, H.-y. Yu, X.-n. Li and J.-g. Wang, *Phys. Chem. Chem. Phys.*, 2012, **14**, 16654.
- 36 Q. Yuan, Z. Zhou, J. Zhuang and X. Wang, *Chem. Commun.*, 2010, **46**, 1491.
- 37 W. He, X. Wu, J. Liu, K. Zhang, W. Chu, L. Feng, X. Hu, W. Zhou and S. Xie, *J. Phys. Chem. C*, 2009, **113**, 10505.
- 38 C. Xu, X. Wang and J. Zhu, *J. Phys. Chem. C*, 2008, **112**, 19841.
- 39 P. Yu, M. Pemberton and P. Plasse, *J. Power Sources*, 2005, **144**, 11.
- 40 J. R. Salgado, E. Antolini and E. R. Gonzalez, *J. Power Sources*, 2005, **141**, 13.
- 41 H. Atae-Esfahani, L. Wang, Y. Nemoto and Y. Yamauchi, *Chem. Mater.*, 2010, **22**, 6310.
- 42 S. Guo, Y. Fang, S. Dong and E. Wang, *J. Phys. Chem. C*, 2007, **111**, 17104.
- 43 S. Guo, S. Dong and E. Wang, *J. Phys. Chem. C*, 2009, **113**, 5485.
- 44 M. Haruta, T. Kobayashi, H. Sano and N. Yamada, *Chem. Lett.*, 1987, 405.
- 45 M. Chen and D. W. Goodman, *Chem. Soc. Rev.*, 2008, **37**, 1860.
- 46 See also the articles in the special issue dedicated to chemistry of nanogold in *Chem Soc Rev*, 2008 **37**.
- 47 M. Valden, X. Lai and D. W. Goodman, *Science*, 1998, **281**, 1647.

- 
- 48 D. R. Rolison, *Science*, 2003, **299**, 1698.
- 49 M. Chen and D. Goodman, *Science*, 2004, **306**, 252.
- 50 D. Cameron, R. Holliday and D. Thompson, *J. Power Sources*, 2003, **118**, 298.
- 51 M. Haruta, N. Yamada, T. Kobayashi and S. Iijima, *J. Catal.*, 1989, **115**, 301.
- 52 G. R. Bamwenda, S. Tsubota, T. Nakamura and M. Haruta, *Catal. Lett.*, 1997, **44**, 83.
- 53 R. Burch, *Phys. Chem. Chem. Phys.*, 2006, **8**, 5483.
- 54 J. A. Rodriguez, P. Liu, J. Hrbek, J. Evans and M. Perez, *Angew. Chem. Int. Ed.*, 2007, **46**, 1329.
- 55 S. Guo, Y. Fang, S. Dong and E. Wang, *J. Phys. Chem. C*, 2007, **111**, 17104.
- 56 Y. Zhang, Q. Huang, Z. Zou, J. Yang, W. Vogel and H. Yang, *J. Phys. Chem. C*, 2010, **114**, 6860.
- 57 Y. Jin, Y. Shen and S. Dong, *J. Phys. Chem. B*, 2004, **108**, 8142.
- 58 S. Guo, L. Wang, S. Dong and E. Wang, *J. Phys. Chem. C*, 2008, **112**, 13510.
- 59 S. Guo, S. Dong and E. Wang, *J. Phys. Chem. C*, 2008, **112**, 2389.
- 60 J. Zeng, J. Yang, J. Y. Lee and W. Zhou, *J. Phys. Chem. B*, 2006, **110**, 24606.
- 61 X. Ge, R. Wang, P. Liu and Y. Ding, *Chem. Mater.*, 2007, **19**, 5827.
- 62 J. Luo, P. N. Njoki, Y. Lin, L. Wang and C. J. Zhong, *Electrochem. Commun.*, 2006, **8**, 581.
- 63 J. Luo, P. N. Njoki, Y. Lin, D. Mott, L. Wang and C.-J. Zhong, *Langmuir*, 2006, **22**, 2892.
- 64 J. Luo, M. M. Maye, V. Petkov, N. N. Kariuki, L. Wang, P. Njoki, D. Mott, Y. Lin and C.-J. Zhong, *Chem. Mater.*, 2005, **17**, 3086.
- 65 W. Tang, S. Jayaraman, T. F. Jaramillo, G. D. Stucky and E. W. McFarland, *J. Phys. Chem. C* 2009, **113**, 5014.
- 66 J. Luo, M. M. Maye, N. N. Kariuki, L. Wang, P. Njoki, Y. Lin, M. Schadt, H. R. Naslund and C.-J. Zhong, *Catal. Today*, 2005, **99**, 291.
- 67 J. Zhang, K. Sasaki, E. Sutter and R. Adzic, *Science*, 2007, **315**, 220.
- 68 A. Bruix, J. A. Rodriguez, P. J. Ramirez, S. D. Senanayake, J. Evans, J. B. Park, D. Stacchiola, P. Liu, J. Hrbek and F. Illas, *J. Amer. Chem. Soc.*, 2012, **134**, 8968.
- 69 J.A. Rodriguez and F. Illas, *Phys. Chem. Chem. Phys.*, 2012, **14**, 427.
- 70 J. A. Rodriguez, P. J. Ramirez, G. G. Asara, F. Viñes, J. Evans, P. Liu, J. M. Ricart, F. Illas, *Angew. Chem. Int. Ed.*, 2014, **53**, 11270.
- 71 A. Hirsch, *Nature Materials*, 2010, **9**, 868.
- 72 F. Diederich and M. Kivala, *Advanced Materials*, 2010, **22**, 803.

- 
- 73 E. Antolini, *Appl. Catal., B*, 2009, **88**, 1.
- 74 T. Li and P. B. Balbuena, *J. Phys. Chem. B*, 2001, **105**, 9943.
- 75 I. Fampiou and A. Ramasubramaniam, *J. Phys. Chem. C*, 2014, **116**, 6543.
- 76 D. Cakir and O. Gulseren, *J. Phys. Chem. C*, 2014, **116**, 5735.
- 77 N. T. Cuong, A. Sugiyama, A. Fujiwara, T. Mitani and D. H. Chi, *Phys. Rev. B: Condens. Matter*, 2009, **79**, 235417.
- 78 T. Yumura, K. Kimura, H. Kobayashi, R. Tanaka, N. Okumura and T. Yamabe, *Phys. Chem. Chem. Phys.*, 2009, **11**, 8275.
- 79 J. Akola and H. Hakkinen, *Phys. Rev. B: Condens. Matter*, 2006, **74**, 165404.
- 80 G. Chen, S. J. Li, Y. Su, V. Wang, H. Mizuseki and Y. Kawazoe, *J. Phys. Chem. C*, **115**, 2014, 20168.
- 81 C. Sikorska and P. Skurski, *Chem. Phys. Lett.*, 2012, **536**, 34.
- 82 M. Zhou, A. Zhang, Z. Dai, Y. P. Feng and C. Zhang, *J. Phys. Chem. C*, 2014, **114**, 16541.
- 83 A. Roldán, S. González, J. M. Ricart and F. Illas, *Chem. Phys. Chem.*, 2009, **10**, 348.
- 84 A. Roldán, J. M. Ricart and F. Illas, *Theoret. Chem. Acc.*, 2011, **128**, 675.
- 85 Y.-H. Fang and Z.-P. Liu, *J. Phys. Chem. C*, 2014, **115**, 17508.
- 86 E. Christoffersen, P. Liu, A. Ruban, H. L. Skriver and J. K. Nørskov, *J. Catal.*, 2001, **199**, 123.
- 87 O. Uzengi Akturk and M. Tomak, *Phys. Rev. B: Condens. Matter*, 2009, **80**, 085417.
- 88 J. P. Perdew, K. Burke, M. Ernzerhof, *Phys. Rev. Lett.*, 1996; **77**, 3865.
- 89 P. Giannozzi, S. Baroni, N. Bonini, M. Calandra, CCR. Car, D. Ceresoli, et al., *J. Phys. Condens Matter*, 2009; **21**, 395502.
- 90 P. Janthon, S. M. Kozlov, F. Vines, J. Limtrakul, F. Illas, *J. Chem. Theory. Comput.*, 2013; **9**, 1631.
- 91 D. Vanderbilt, *Phys. Rev. B*, 1990; **41**, 7892.
- 92 W. E. Pickett, *Comput. Phys. Rep.*, 1989; **9**, 115.
- 93 E. Yeager, Electrocatalysts for O<sub>2</sub> reduction, *Electrochim. Acta* **1984**, *29*, 1527-1537.
- 94 M. R. Terasevich, A. Sadkowski, E. Yeager, *Comprehensive Treatise of Electrochemistry*, edited by B. Conway, J. M. Bockris, E. Yeager, S. U. M. Khan, R. E. White (Plenum, New York, **1983**), Vol. 7, p. 301
- 95 J. Lipkowsky, P. N. Ross, *Electrocatalysis*, Wiley-VCH, Inc., 1998. p. 199.
- 96 J. Li, H. Li, X. Liang, Sh. Zhang, T. Zhao, D. Xia and Z. Wu, *J Phys Chem A.*, 2009; **113**, 791.

- 
- 97 JW. Zheng, SML. Nai, MF. Ng, P. Wu, J. Wei and M. Gupta, *J Phys Chem C*, 2009, **113**, 14015.
- 98 J. Wang, G. Wang and J. Zhao, *Phys. Rev. B: Condens. Matter*, 2002, **66**, 035418.
- 99 L. Xiao, B. Tollberg, X. Hu and L. Wang, *J. chem. Phys.*, 2006, **124**, 114309.
- 100 B. Assadollahzadeh and P. Schwerdtfeger, *J. chem. Phys.*, 2009, **131**, 064306.
- 101 A. Walker, *J. chem. Phys.*, 2005, **122**, 094310.
- 102 S. J. Wang, X. Y. Kuang, C. Lu, Y. F. Li and Y. R. Zhao, *Phys. Chem. Chem. Phys.*, 2011, **13**, 10119.
- 103 L. Cheng, K. Xiao-Yu, L. Zhi-Wen, M. Ai-Jie and M. Yan-Ming, *J. Phys. Chem. A*, 2011, **115**, 9273.
- 104 L. Xiao and L. Wang, *J. Phys. Chem. A*, 2004, **108**, 8605.
- 105 K. Bhattacharyya and C. Majumder, *Chem. Phys. Lett.*, 2007, **446**, 374.
- 106 V. Kumar and Y. Kawazoe, *Phys. Rev. B: Condens. Matter*, 2008, **77**, 205418.
- 107 M. Huda, M. K. Niranjana, B. Sahu and L. Kleinman, *Phys. Rev. A: At. Mol. Opt. Phys.*, 2006, **73**, 053201.
- 108 A. Sebetci, *Phys. Chem. Chem. Phys.*, 2009, **11**, 921.
- 109 T. Futschek, J. Hafner and M, *J. Phys.: Condens. Matter*, 2006, **18**, 9703.
- 110 C. Song, Q. Ge and L, *J. Phys. Chem. B*, 2005, **109**, 22341.
- 111 Y. K. Chen, W. Q. Tian and Y. A. Wang, *Int. J. Quantum Chem.*, 2012, **112**, 65.
- 112 X. Kuang, X. Wang and G. Liu, *Eur. Phys. J. D*, 2011, **63**, 111.
- 113 D. Yuan, Y. Wang and Z. Zeng, *J. chem. Phys.*, 2005, **122**, 114310.
- 114 F. Wang, P. Liu and D. Zhang, *J. Mol. Model.*, 2011, **17**, 1069.
- 115 C. Majumder and S. Kulshreshtha, *Phys. Rev. B: Condens. Matter*, 2006, **73**, 155427.
- 116 Y.-A. Lv, Y.-H. Cui, X.-N. Li, X.-Z. Song, J.-G. Wang and M. Dong, *Physica E*, 2010, **42**, 1746.
- 117 Z. Li, Z.-X. Chen, G.-J. Kang and X. He, *Catal. Today*, 2011, **165**, 25.
- 118 M. Amft, B. Sanyal, O. Eriksson and N. V. Skorodumova, *J. Phys.: Condens. Matter*, 2011, **23**, 205301.
- 119 G. M. Wang, J. J. BelBruno, S. D. Kenny and R. Smith, *Phys. Rev. B: Condens. Matter*, 2004, **69**, 195412.
- 120 J. G. Wang, Y. Lv, X. Li and M. Dong, *J. Phys. Chem. C*, 2008, **113**, 890.
- 121 K. E. Hayes and H.-S. Lee, *Chem. Phys.*, 2012, **393**, 96.
- 122 H. C. Dam, N. T. Cuong, A. Sugiyama, T. Ozaki, A. Fujiwara, T. Mitani and S. Okada, *Phys. Rev. B: Condens. Matter*, 2009, **79**, 115426.

- 
- 123 I. Fampiou and A. Ramasubramaniam, *J. Phys. Chem. C*, 2012, **116**, 6543.
- 124 G. Henkelman, A. Arnaldsson and H. Jónsson, *J. Comput. Chem.*, 2006, **36**, 354.
- 125 E. Sanville, S. D. Kenny, R. Smith and G. Henkelman, *J. Comput. Chem.*, 2007, **28**, 899.
- 126 R. Varns and P. Strange, *J. Phys.: Condensed Matter*, 2008, 20, 225005.
- 127 J. Wu, S. W. Ong, H. C. Kang and E. S. Tok, *J. Phys. Chem. C*, 2010, **114**, 21252.
- 128 D. Çakir and O. Gülseren, *J. Phys. Chem. C*, 2012, **116**, 5735.
- 129 E. M. Fernandez, P. Ordejon and L. C. Balbas, *Chem. Phys. Lett.*, 2005, **408**, 252.
- 130 A. Lyalin and T. Taketsugu, *J. Phys. Chem. C*, 2009, **113**, 12930.
- 131 A. Lyalin and T. Taketsugu, *J. Phys. Chem. Lett.*, 2010, **1**, 1752.
- 132 G. Mills, M. S. Gordon and H. Metiu, *Chem. Phys. Lett.*, 2002, **359**, 493.
- 133 X. Lin, N. J. Ramer, A. M. Rappe, K. C. Hass, W. F. Schneider and B. L. Trout, *J. Phys. Chem. B*, 2001, **105**, 7739.
- 134 M. Chen, S. Bates, R. Van Santen and C. Friend, *J. Phys. Chem. B*, 1997, **101**, 10051.
- 135 A. Roudgar, M. Eikerling and R. van Santen, *Phys. Chem. Chem. Phys.*, 2010, **12**, 614.

